Thermochimica Acta 517 (2011) 16–23

Contents lists available at ScienceDirect

Thermochimica Acta

journal homepage: www.elsevier.com/locate/tca

The effect of mass ratio of electrolyte and electrodes on the thermal stabilities of electrodes used in lithium ion battery

Qingsong Wang[a,*], Ping Ping[a], Jinhua Sun[a,**], Chunhua Chen[b]

[a] State Key Laboratory of Fire Science, University of Science and Technology of China, Hefei 230026, PR China
[b] Department of Materials Science & Engineering, University of Science and Technology of China, Hefei 230026, PR China

ARTICLE INFO

Article history:
Received 2 September 2010
Received in revised form
25 December 2010
Accepted 19 January 2011
Available online 26 February 2011

Key words:
Lithium ion battery
Mass ratio
Thermal behavior
Deconvolution

ABSTRACT

The mass ratio between electrode and electrolyte in lithium-ion battery plays a key role for the battery thermal stability. Its effect on the thermal stability of their coexisting system was studied using C80 microcalorimeter. For the $Li_{0.5}CoO_2$–$LiPF_6$/ethylene carbonate (EC) + diethyl carbonate (DEC) coexisting system, when the mass ratios of $Li_{0.5}CoO_2$–$LiPF_6$/EC + DEC are 2:1, 1:1, 1:2 and 1:3, one, two, three and four main exothermic peaks are detected with total heat generation of $-1043.8\,J\,g^{-1}$, $-1052.6\,J\,g^{-1}$, $-1178.5\,J\,g^{-1}$ and $-1684.5\,J\,g^{-1}$, respectively. For the Li_xC_6–$LiPF_6$/EC + DEC coexisting system, the thermal behavior trend is similar, and the heat generation increases with the electrolyte content increasing, however, and the onset temperature are very close to each others. The heating rate also influence the heat generation rate for the two coexisting system, too far or too low heating rate could results in varies heat generation.

1. Introduction

Lithium-ion batteries are very common in portable consumer electronics because of their high energy-to-weight ratios, lack of memory effect, and slow self-discharge when not in use. In addition to consumer electronics, lithium-ion batteries are increasingly used in automotive, and aerospace applications due to their high energy density [1]. However, certain kinds of mistreatment may cause conventional lithium ion batteries to explode. Researchers in industry and academia do not fully understand why lithium ion batteries sometimes catch fire or explode [2]. However, it is commonly thought the possible exothermic reactions are: (1) the chemical reduction of the electrolyte by the anode, (2) the thermal decomposition of the electrolyte, (3) the oxidation of the electrolyte on the cathode, (4) the thermal decomposition of the anode, and (5) the thermal decomposition of the cathode [3–7]. The anode and cathode react with electrolyte play a key role in causing the thermal accumulation inner the lithium ion battery.

The thermal stability or the thermal behavior of lithium-ion battery has been widely investigated by differential scanning calorimetry (DSC), accelerating rate calorimetry (ARC) or C80 [5–16]. The thermal behaviors of lithium nickel oxide [8,17–19], lithium manganese oxide [20–22], and lithium cobalt oxide [13,16,23,24], as the cathode materials of the lithium-ion battery, have been investigated. $LiCoO_2$ is one of the widely used cathode materials for lithium ion cells, and its thermal stability was widely studied. The related result reveals that Li_xCoO_2 shows two exothermic peaks, one begins at 190 °C and another one begins at 290 °C detected by DSC [25]. By using C80, $Li_{0.5}CoO_2$ starts to release heat at 170 °C, and reaches to peak temperature at 256 °C [16]. The difference may be caused by the accuracy of the calorimeter and the heating rate. C80 can be set at lower heating rate, and then the mild reaction can be detected at early stage. In the presence of sufficient solvent, the reaction proceeds in a clear stepwise manner through solid phases as a function of temperature as $Li_xCoO_2 \rightarrow xLiCoO_2\ 1/3\,(1-x)Co_3O_4 + 1/3\,(1-x)O_2$. Accompanying these changes are solvent combustion reactions due to the evolved oxygen that release large amounts of heat. If there is only a small amount of solvent present relative to the amount of $Li_{0.5}CoO_2$, the latter steps of the reaction do not occur anymore, at least at temperatures below 450 °C [9].

The thermal stability of graphite anode in an electrolyte is controlled by a solid electrolyte interphase (SEI) formed on the lithiated graphite anode surface. The function of this SEI layer is to protect the graphite grains from cointercalation of solvent molecules between the graphite planes, while still permitting the transport of lithium ions. Thermal stability of graphite anode with electrolyte also was widely investigated by DSC, ARC or C80 [11,15,26–31]. In the presence of electrolyte, Yamaki et al. [32] detected a mild heat generation starts from 130 °C with a small peak at 140 °C by using DSC. The mild heat generation continued until a sharp exothermic

* Corresponding author. Tel.: +86 551 360 6455; fax: +86 551 360 1669.
** Corresponding author. Tel.: +86 551 360 6425; fax: +86 551 360 1669.
E-mail addresses: pinew@ustc.edu.cn (Q. Wang), sunjh@ustc.edu.cn (J. Sun).

0040-6031/$ – see front matter © 2011 Elsevier B.V. All rights reserved.
doi:10.1016/j.tca.2011.01.015

peak appears at 280 °C. The peak at 140 °C seems caused by the reaction (SEI formation) of the electrolyte and lithiated graphite. The peak at 280 °C is probably a direct reaction of lithiated graphite and electrolyte by a breakdown of SEI [32]. Choi et al. [33] detected three exothermic peaks at 90 °C, 270 °C and 325 °C of the lithiated graphite and electrolyte, respectively, by using DSC as well. C80 results show that single Li_xC_6 has one exothermic peak, which is attributed to the SEI decomposition. Four exothermic peaks were detected in Li_xC_6–1.0 M $LiPF_6$/ethylene carbonate (EC) + diethyl carbonate (DEC) electrolyte. These four peaks are attributed to SEI decomposition(100 °C), Li-electrolyte reaction as well as new SEI film formation (213 °C), new SEI film decomposition(229 °C), and lithium metal with PVDF/other products reactions(246 °C) [7].

The core materials in a lithium ion battery are cathode, anode and electrolyte, however, different designs and capacities are proposed by different manufacturers, and one manufacturer may offer variations. Their mass ration is also varying for different active materials and different capacity cells. For example, in a 10 Ah cell, the mass ratio among anode, cathode and electrolyte is 11:56:33, for a 100 Ah cell, the ratio changes to 22:54:24 [34]. The thermal stability of cathode and anode electrodes at different state of charge was investigated with and without the presence of electrolyte. It was concluded that the electrode reacts with electrolyte at elevated temperature, and then, the mass ratio of the electrode and electrolyte influences the reaction and heat generation, which is important to the safe use of the lithium ion battery. Therefore, the mass ratio effects of $Li_{0.5}CoO_2$ cathode and lithiated graphite anode (Li_xC_6) with 1.0 M $LiPF_6$/EC + DEC electrolyte on theirs thermal stability were studied by using C80 micro-calorimeter in this work.

2. Experimental

The organic solvents are commercially available products made by Zhangjiagang Guotai-Huarong Co., Ltd. with the water content below 20 ppm. The salt $LiPF_6$ was produced by Tianjin Jinniu Co., Ltd. with the water content below 20 ppm. From these chemicals, the electrolyte of 1.0 M $LiPF_6$/EC + DEC (1:1 wt.%) were prepared in argon-filled glove box (MBraun Labmaster 130, <1 ppm O_2 and H_2O). $LiCoO_2$ was produced by Tianjin Bamo Co., Ltd. The composition of the cathode was 84% of $LiCoO_2$, 8% of acetylene black, and 8% of polyvinylidene fluoride (PVDF) binder. The graphite electrode is made of 92% graphite material (Hongyuan Carbon Industry Co., Ltd) and 8% PVDF binder, coat on copper foil. The electrodes were dried over night in vacuum at 70 °C and handled in an argon filled glove box. The electrodes were cut as a 14 mm diameter disk with 400 μm thickness, and then the batteries assembled by these disks could provide more mass from one sample for C80 experiment.

CR2032 coin cells were assembled in an argon-filled glove box with the $LiCoO_2$ or graphite as positive electrode, lithium as counter electrode, 1.0 M $LiPF_6$/EC + DEC as the electrolyte and Celgard 2400 polyethylene as the separator (20 μm thickness). The $LiCoO_2$/Li cells were galvanostatically cycled three times on a multi-channel battery cycler (Neware BTS-6V10 mA, Shenzhen) at room temperature, between 4.2 V and 2.8 V at 0.2 mA cm^{-2} current density. After obtaining 4.2 V, a signature-charge test (equivalent to constant voltage charging) was used to stabilize the electrode at the desired voltage. The C/Li half cells were galvanostatically cycled three times on a multi-channel battery cycler (Neware BTS-6V10 mA, Shenzhen) at 0.2 mA cm^{-2} current density. The C/Li cells were "discharged" to 3.0 V and then "charged" to 0 V. The definition of "discharge" here is for the half-cells, namely the lithiation process for the graphite electrodes. If they are used as the anodes in full cells, this process corresponds to the "charge" step. Then, the C/Li half cells were "charged" to 0 V by using constant current condition, and kept on discharging 2 h at 0 V.

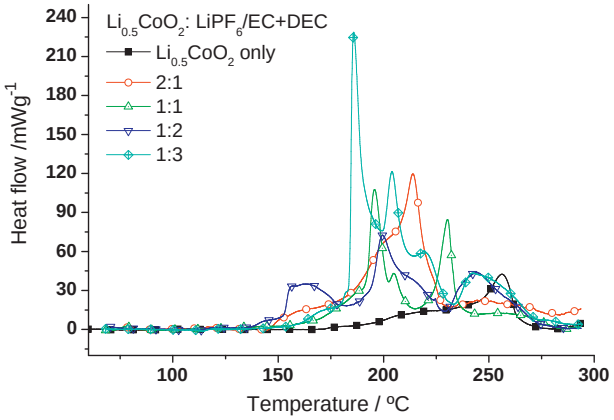

Fig. 1. Thermal behaviors of $Li_{0.5}CoO_2$–1.0 M $LiPF_6$/EC + DEC coexisting systems with different mass ratio.

Then the charged $LiCoO_2$/Li cells and "charged" C/Li cells were disassembled in glove box. To remove the electrolyte from the electrode, the wet charged electrode powder was placed into a bottle. A volatile organic solvent of dimethyl carbonate (DMC) was added to that bottle and then the bottle was shaken by hand. The sample was then decanted and the DMC rinsing procedure was repeated. After the second decanting, the sample was dried to remove the DMC solvent. After drying, the electrode material was scraped, trying not to abrade the film, from the current collectors carefully for thermal test.

The electrode was weighted and transferred into a high-pressure stainless steel vessel (8.5 ml in volume) of C80 micro-calorimeter. A small burette was used to drop the electrolyte into the vessel with certain mass controlled by electronic balance and scale on the burette. After that, the vessel was sealed in argon atmosphere. The samples were then moved from the glove box and analyzed in the C80 experiment. The weight of each sample (vessel + sample) was measured before and after the experiment to verify that the system was hermetically sealed. The weight was constant in all cases, indicating that there were no leaks during the experiments. The measurements were carried out using a heating rate set at 0.2 °C min^{-1} in the temperature range 30–300 °C in argon filled vessel. The thermal behavior of each sample with temperature was thus recorded automatically, and the C80 calculations were based on dry film weight of the electrode material.

3. Results and discussion

3.1. Mass ratio effect on the thermal stability of $Li_{0.5}CoO_2$-electrolyte coexisting system

Fig. 1 is the heat flow plots of $Li_{0.5}CoO_2$–1.0 M $LiPF_6$/EC + DEC coexisting systems at different mass ratios. In Fig. 1, the single $Li_{0.5}CoO_2$ starts to release heat at 170 °C, and an exothermic shoulder at about 220 °C was observed and reaches to main peak temperature at 256 °C with reaction heat of −411.5 J g^{-1}. The shoulder probably caused by the phase transition from the layered rock-salt to the spinel structure based on Baba's result [5], and the main peak is the decomposing of $Li_{0.5}CoO_2$ with O_2 releasing. When the mass ratio between $Li_{0.5}CoO_2$ and electrolyte is 2:1, it starts to release heat at 146 °C, and reaches to the peak temperature at 214 °C with the total heat generation of −1043.8 J g^{-1}. Before and after this peak, two shoulder exothermic peaks were found in the heat flow plot at 200 °C and 244 °C, respectively, which means some exothermic reactions couple together. The dominate reactions in this case are lowered to 214 °C, which is probably a decomposition of solvent caused by active surface of the delithi-

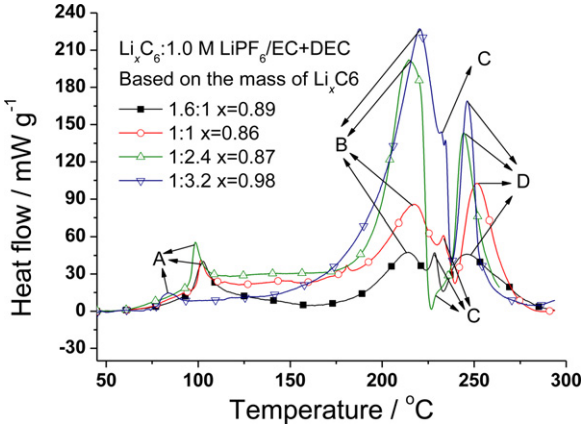

Fig. 2. Thermal behaviors of Li_xC_6–1.0 M $LiPF_6$/EC + DEC coexisting systems with different mass ratio, and the heat flow are based on electrode.

ated $Li_{0.5}CoO_2$ [35]. With the increasing of electrolyte content in the coexisting system, the exothermic processes increase correspondingly. When the mass of $Li_{0.5}CoO_2$ is equal to the mass of electrolyte, two central exothermic peaks and a shoulder exothermic peak in the main reaction processes were detected. Moreover, there is a small exothermic peak at 78 °C in $Li_{0.5}CoO_2$–$LiPF_6$/EC + DEC system. This mild exothermic process is considered as the decomposition of SEI formed on the cathode surface. With the temperature elevating, the $Li_{0.5}CoO_2$–1.0 M $LiPF_6$/EC + DEC system starts to release heat at 128 °C and reaches to exothermic peak temperatures at 196 °C, 205 °C and 230 °C with total heat generation of −1052.6 J g^{-1}. In an open system, that is the outer oxygen involves the reaction, more heat will be generated, which is proved by Huang et al. [36] using oxygen bomb calorimeter for $Li_{0.5}CoO_2$–$LiPF_6$/EC + DEC. The first two peaks are from combustion of solvent with oxygen from the reduction of $Li_{0.5}CoO_2$ to Co_3O_4, and the last peaks maybe due to Co_3O_4 decompose to CoO at elevated temperature [23]. When the mass ratio of $Li_{0.5}CoO_2$ with electrolyte is 1:2, three obvious exothermic processes were detected with the peak temperatures locate as 163 °C, 200 °C and 244 °C, respectively, and the total heat generation is −1178.5 J g^{-1}. When the mass ratio of $Li_{0.5}CoO_2$ with electrolyte is 1:3, except the exothermic peaks locate at 186 °C, 204 °C and 242 °C, another small exothermic peak temperature at 219 °C was detected. The biggest one locates at 186 °C among the four peaks, and the total heat generation is −1684.5 J g^{-1}. When the electrolyte mass is not less than $Li_{0.5}CoO_2$ mass, it undergoes similar thermal reactions as stated when the mass ratio is 1:1 [9]. It also can be seen that when the masses of $Li_{0.5}CoO_2$ and electrolyte are close to each other, the heat generation are close too. If the mass difference is large, such as the mass ratio $Li_{0.5}CoO_2$ with electrolyte is 1:3, the heat generation increased 631.9 J g^{-1} than that of the mass ratio is 1:1. The increased heat generation may be contributed by the thermal decomposition of the superfluous electrolyte. Therefore, it is better to use fewer electrolytes at the condition of satisfying the electrochemical performance of the lithium ion battery, which will reduce the active substance and enhance the thermal stability of the battery.

3.2. Mass ratio effect on the thermal stability of Li_xC_6-electrolyte coexisting system

Fig. 2 shows the thermal behavior of Li_xC_6–1.0 M $LiPF_6$/EC + DEC at 1.6:1, 1:1, 1:2.4 and 1:3.2 mass ratios, respectively. The Li_xC_6-electrolyte systems show varying thermal behaviors at different Li_xC_6-electrolyte mass ratios. It should be noted that the heat generation was calculated based on the mass of Li_xC_6. In Fig. 2 all the samples show similar thermal behavior at elevated temperature. However, the exothermic peaks are overlapped together and hard to analysis the reaction processes. As the deconvolution method is a good method to pick the peaks from the overlapped peaks [37,38], and was used here to separate the peaks. The deconvoluted plots were shown from Fig. 3 to Fig. 6 for the mass ratio of Li_xC_6 and electrolyte at 1.6:1, 1:1, 1:2.4 and 1:3.2, respectively.

Before deconvolution, there are three obvious peaks can be identified and are designated as peak A, B, and D in Fig. 2. A faint peak between peak B and peak D appears in some cases, and it couples with other process and is designated peak C for unification. After deconvolution, two more exothermic peaks are picked from the plots, which are designated as peak e and f. The other original four peaks use lowercase letters a–d corresponding to the original four peaks A–D, respectively. Based on the previous study [7], the peaks A–D are attributed to the SEI breakdown, lithium-electrolyte reaction, new SEI film breakdown, and Li_2CO_3 formation reactions overlapped with PVDF reactions, respectively. As the trace water in the electrolyte could reacts with $LiPF_6$ to produce the HF, and again, the HF will react with $ROCO_2Li$ and $LiCO_3$, which are formed in the SEI films. The reactions processes are as followings [39,40]:

$$H_2O + LiPF_6 \rightarrow POF_3 + LiF + 2HF$$

$$ROCO_2Li + HF \rightarrow ROCO_2H + LiF$$

$$Li_2CO_3 + 2HF \rightarrow H_2O + CO_2 + 2LiF$$

The new produced water will further react with $LiPF_6$ and repeat the above reactions. Therefore, the water in the electrolyte will reduce the thermal stability of SEI film formed on the graphite anode. The first exothermic peak A in the Fig. 2 not only decomposes itself, but also is speeded by the trace water in the electrolyte. Lewis acid of PF_5 react with the oxygen atom of carbonyl groups (–C═O) and causes the destruction of the SEI layer. The intercalated lithium reacted with the electrolyte to form a new stable SEI film after SEI decomposition. This new SEI film decomposes again with temperature rising [7].

In the deconvoluted plots, the peaks e shows a very slowly process, it is thought the process of embedded lithium ion deintercalated from the graphite layer. Another peak f is thought the electrolyte decomposition process by comparing with the previous study[41]. When the mass ratio of $Li_{0.89}C_6$–1.0 M $LiPF_6$/EC + DEC is 1.6:1, it starts to release heat at 57 °C and reaches the first peak at 103 °C. The B, C and D peaks locate at 214 °C, 228 °C and 246 °C, respectively, with the total heat generation of −1298.7 J g^{-1}. The corresponding deconvoluted plot peaks almost keep at the same locations, another two peaks e and f are locate at 116.0 °C and 197.9 °C. However, the total heat generation of −1271.0 J g^{-1} closes to the original one. All the other thermodynamic parameters are listed in Table 1. At 1:1 mass ratio, the coexisting system starts to release heat at 60 °C, followed by four exothermic peaks at 102 °C, 218 °C, 233 °C and 252 °C, respectively, with total heat generation of −2342.4 J g^{-1}. Another two peaks at 156.7 °C and 181.6 °C were discovered in the deconvoluted plot in Fig. 4, and Table 2 lists more detailed results. With the mass of electrolyte increasing in the coexisting system, at 1:2.4 mass ratio, the onset temperature is 57 °C, peaks A, B and D locate at 99 °C, 215 °C and 246 °C, while the third exothermic peak C is too small to be recognized. The total heat generation increases to −3100.6 J g^{-1}, which is higher than the former two cases. However, the peak C is clearly displayed in the deconvoluted plot in Fig. 5, it is locates at 243.3 °C, but the heat generation is quite small, only 54.9 J g^{-1} in Table 3. When the mass ratio of $Li_{0.98}C_6$–1.0 M $LiPF_6$/EC + DEC is 1:3.2, the onset temperature is very close to the other cases, but the peak A is lower to 83 °C and the rest three exothermic peaks are 220 °C, 232 °C, and 246 °C, respectively, which are close to the other cases. The total heat gen-

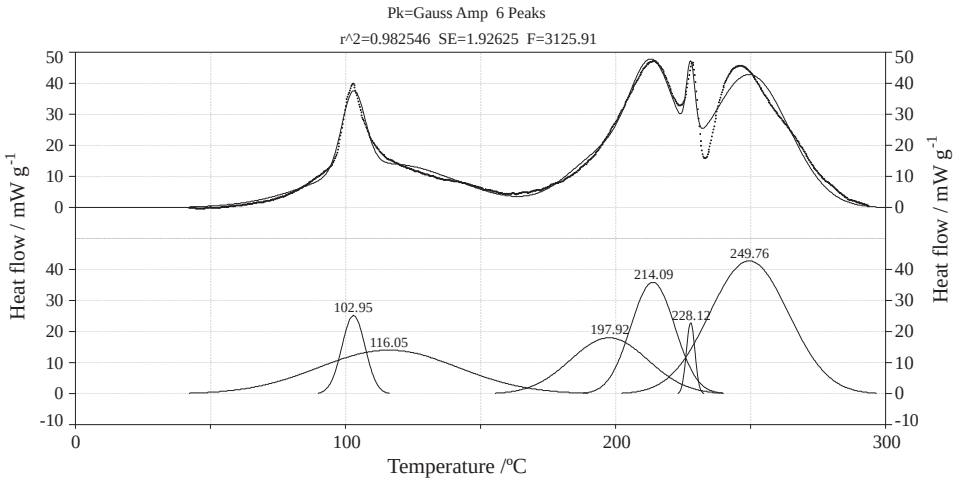

Fig. 3. Deconvoluted C80 plots of heat flow as a function of temperature for Li_xC_6 and 1.0 M $LiPF_6$/EC + DEC electrolyte at 1.6:1 mass ratio.

Table 1
Thermodynamics and kinetics of Li_xC_6 and 1.0 M $LiPF_6$/EC + DEC electrolyte at 1.6:1 mass ratio.

Li_xC_6-electrolyte 1.6:1 mass ratio	Peak temp. (°C)	Reaction heat (J g^{-1})	Activation energy E (kJ mol^{-1})	Pre-exponential factor A (s^{-1})	Relativity R^2
Peak a	103.0	−81.5	265.26	2.12×10^{33}	0.9719
Peak e	116.0	−275.5	74.33	1.99×10^{6}	0.99617
Peak f	197.9	−195.4	193.41	7.04×10^{17}	0.9844
Peak b	214.1	−220.1	356.23	6.50×10^{34}	0.98535
Peak c	228.1	−27.0	785.72	6.41×10^{78}	0.96408
Peak d	249.8	−471.5	249.88	2.84×10^{21}	0.98911
Total		−1271			

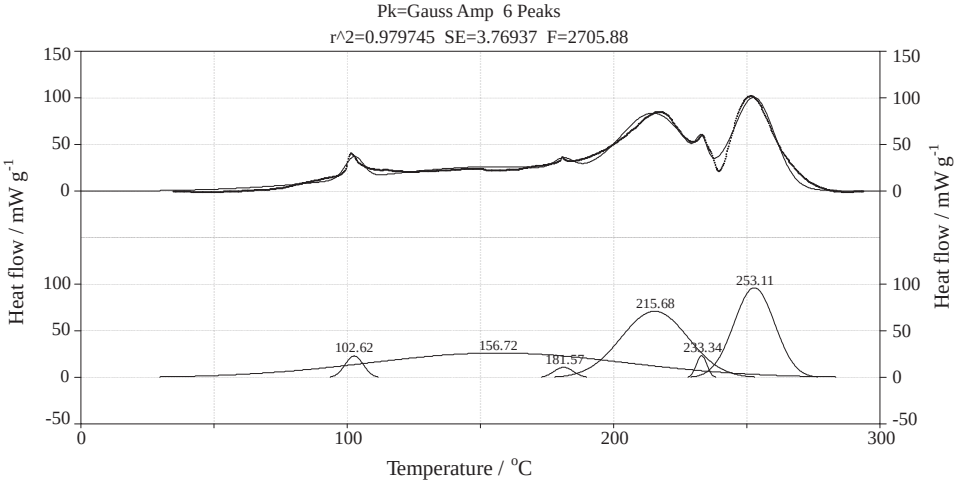

Fig. 4. Deconvoluted C80 plots of heat flow as a function of temperature for Li_xC_6 and 1.0 M $LiPF_6$/EC + DEC electrolyte at 1:1 mass ratio.

Table 2
Thermodynamics and kinetics of Li_xC_6 and 1.0 M $LiPF_6$/EC + DEC electrolyte at 1:1 mass ratio.

Li_xC_6-electrolyte 1:1 mass ratio	Peak temp. (°C)	Reaction heat (J g^{-1})	Activation energy E (kJ mol^{-1})	Pre-exponential factor A (s^{-1})	Relativity R^2
Peak a	102.6	−60.2	439.31	7.46×10^{57}	0.96379
Peak e	156.7	−963.4	38.28	3.64×10^{0}	0.99965
Peak f	181.6	−30.8	551.47	1.46×10^{60}	0.98567
Peak b	215.7	−671.0	280.37	4.74×10^{26}	0.99399
Peak c	233.3	−34.7	454.21	4.33×10^{43}	0.8471
Peak d	253.1	−552.8	403.11	3.82×10^{36}	0.98387
Total		−2312.9			

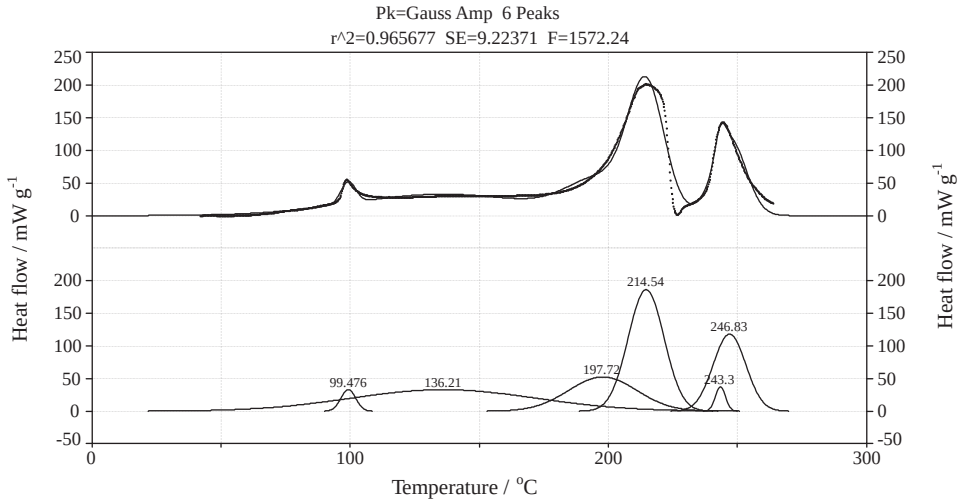

Fig. 5. Deconvoluted C80 plots of heat flow as a function of temperature for Li_xC_6 and 1.0 M $LiPF_6$/EC + DEC electrolyte at 1:2.4 mass ratio.

Table 3
Thermodynamics and kinetics of Li_xC_6 and 1.0 M $LiPF_6$/EC + DEC electrolyte at 1:2.4 mass ratio.

Li_xC_6-electrolyte 1:2.4 mass ratio	Peak temp. (°C)	Reaction heat (J g^{-1})	Activation energy E (kJ mol^{-1})	Pre-exponential factor A (s^{-1})	Relativity R^2
Peak a	99.5	−70.8	520.84	8.82×10^{69}	0.97489
Peak e	136.2	−882.0	47.30	9.51×10^{2}	0.99452
Peak f	197.7	−522.2	214.97	2.30×10^{20}	0.99256
Peak b	214.5	−971.8	448.93	7.20×10^{44}	0.98869
Peak c	243.3	−54.9	991.09	1.49×10^{97}	0.96459
Peak d	246.8	−560.5	492.67	1.50×10^{46}	0.98593
Total		−3062.2			

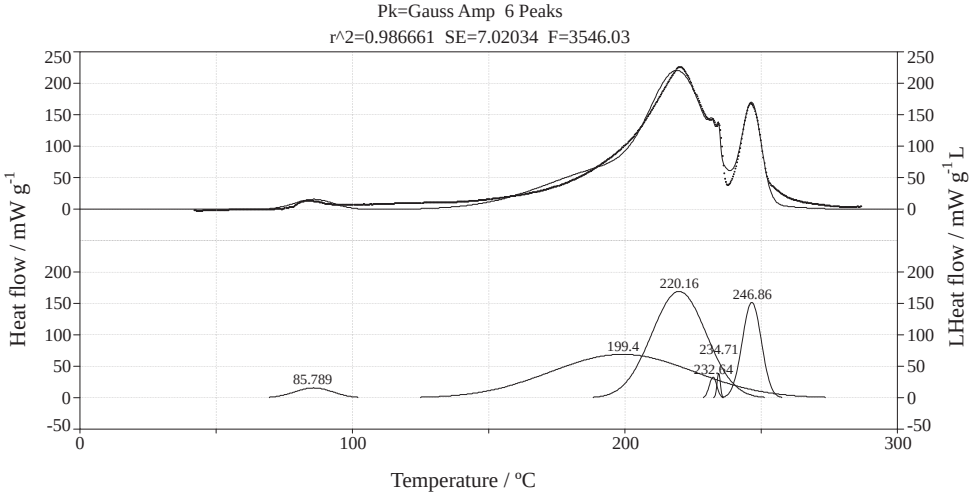

Fig. 6. Deconvoluted C80 plots of heat flow as a function of temperature for Li_xC_6 and 1.0 M $LiPF_6$/EC + DEC electrolyte at 1:3.2 mass ratio.

Table 4
Thermodynamics and kinetics of Li_xC_6 and 1.0 M $LiPF_6$/EC + DEC electrolyte at 1:3.2 mass ratio.

Li_xC_6-electrolyte 1:3.2 mass ratio	Peak temp. (°C)	Reaction heat (J g^{-1})	Activation energy E (kJ mol^{-1})	Pre-exponential factor A (s^{-1})	Relativity R^2
Peak a	85.8	−86.4	237.59	2.18×10^{31}	0.98817
Peak e	199.4	−1370.8	121.11	7.20×10^{9}	0.99711
Peak b	220.2	−1270.5	327.32	2.19×10^{31}	0.9933
Peak f	232.6	−34.5	1011.97	3.31×10^{101}	0.93675
Peak c	234.7	−17.8	980.61	1.42×10^{98}	0.77992
Peak d	246.9	−395.0	704.53	3.62×10^{67}	0.98124
Total		−3175			

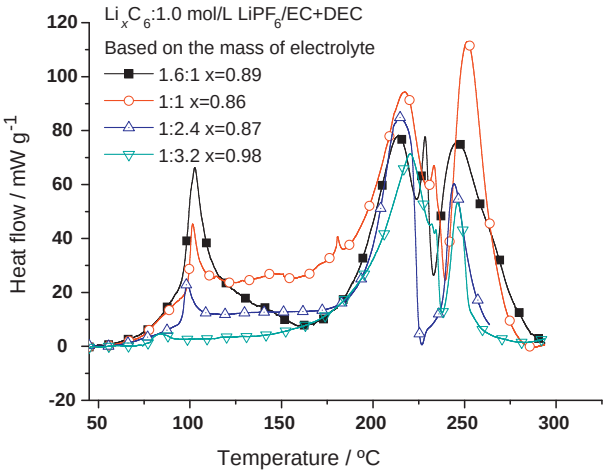

Fig. 7. Thermal behaviors of Li_xC_6–1.0 M $LiPF_6$/EC + DEC coexisting systems with different mass ratio, and the heat flow are based on electrolyte.

eration is −3404.0 J g^{-1}. In the deconvolution plot, two small peaks were fitted at 232.6 °C and 234.7 °C with very little heat generation of −34.5 J g^{-1} and −17.8 J g^{-1}, respectively, as shown in Fig. 6 and Table 4. One of the peaks should be the new formed SEI film breakdown, but it's difficult to clear which one it is.

If the heat generation is integrated based on the mass of Li_xC_6, the heat plots were redrawn in Fig. 7. It can be seen from Fig. 7 that the exothermic peaks are not changed, but the total heat generations are −2077.9 J g^{-1}, −2342.4 J g^{-1}, −1291.9 J g^{-1}, −1063.8 J g^{-1} and −930.6 J g^{-1}, respectively, for the four mass ratios cases. It can be speculated that when the mass ratio is not higher 1:1, the reactions are dominated by electrolyte, and when the mass ration is higher than 1:1, the reactions are dominated by Li_xC_6. It is known based on previous study that decomposition heat of electrolyte is −155 J g^{-1} [42], which is much lower than the reaction heat of coexisting system. When the reaction heat is integrated based on the electrolyte, the heat generation contributed by the superfluous electrolyte decomposition is averaged into the total heat generation, and then, when the mass ratio is higher than 1:1, the total heat generation shows lower than that of mass ration not higher than 1:1.

Assuming the reaction mechanism is dependent on the Arrhenius law, basing on the C80 data, the following Eq. (1) is got as

$$\ln\left(\frac{dH/dt}{\Delta H M_0}\right) = -\frac{E}{R}\frac{1}{T} + \ln A \quad (1)$$

where dH/dt is over all heat flow, ΔH is heat of reaction, M_0 is initial mass of reactant, E is activation energy, R is gas constant, T is temperature of system and A is pre-exponential factor. By plotting the curve of $\ln(dH/dt)/(\Delta H M_0)$ versus inverse temperature, the E and A can be easily calculated.

By using this method, the thermodynamic and kinetics based on the original plots were calculated and listed in Table 5, the thermodynamic and kinetics based on the deconvoluted plots are listed from Table 1 to Table 4. It can be seen that the changes of mass ratio of Li_xC_6 and electrolyte plays less effect on the onset temperature of the Li_xC_6-electrolyte coexisting system, they are start to release heat at the range of 57–60 °C, and the exothermic peaks are almost same except the one at 1:3.2 mass ratio of $Li_{0.98}C_6$–1.0 M $LiPF_6$/EC + DEC. At 1:3.2 mass ratio, the first exothermic peak is 83 °C, this is lower than other three cases, which may be caused by the high content of lithium ion in the Li_xC_6, $x = 9.8$. At 1:1 mass ratio, the third exothermic peak disappears, and it may be emerged with the other reactions, however, the deconvoluted plot discovers the exothermic peak locates at 233.3 °C. The heat

Table 5
Thermodynamic and kinetics parameters of Li_xC_6–1.0 M $LiPF_6$/EC + DEC with different mass ratios.

Li_xC_6:electrolyte	x in Li_xC_6	Onset temp (°C)	Exothermic peak temp (°C)			Reaction heat (J g^{-1})					Activation energy Ez (kJ mol^{-1})		Pre-exponential factor A (s^{-1})		Relativity R^2	
			a	b	c	d	a	b	c	d	Total	Total[a]	a	b	a	b	a	b
1.6:1	0.89	57	103	214	228	246	−344.6	−428.4	−97.0	−428.7	−1298.7	−2077.9	87.0	100.4	1.08×10^8	7.6×10^6	0.997	0.999
1:1	0.86	60	102	218	233	252	−495.5	−1090.6	−138.7	−617.6	−2342.4	−2342.4	78.6	64.3	5.14×10^6	5.9×10^2	0.983	0.998
1:2.4	0.87	57	98	215	–	244	−389.8	−2043.0	–	−667.8	−3100.6	−1291.9	97.2	104.3	5.89×10^9	1.5×10^7	0.974	0.98
1:3.2	0.98	58	83	220	232	246	−66.6	−2490.8	−226.5	−620.1	−3404.0	−1063.8	154.5	54.8	5.74×10^{18}	0.39×10^2	0.979	0.993
1:1[b]	0.84	73	85	211	–	251	−121.3	−616.0	–	−193.3	−930.6	−930.6	130.0	88.2	7.41×10^{14}	7.99×10^5	0.995	0.982

–: No data.
[a] Heat generation based on electrolyte.
[b] Heating rate is 0.5 °C min^{-1}.

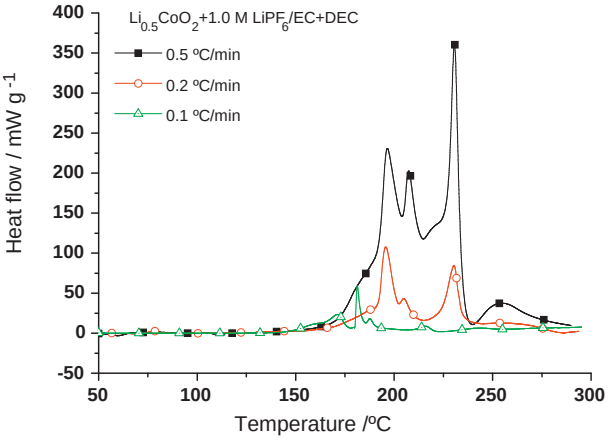

Fig. 8. Heat flows of $Li_{0.5}CoO_2$–1.0 M $LiPF_6$/EC + DEC at 0.5, 0.2 and 0.1 °C min^{-1} heating rate.

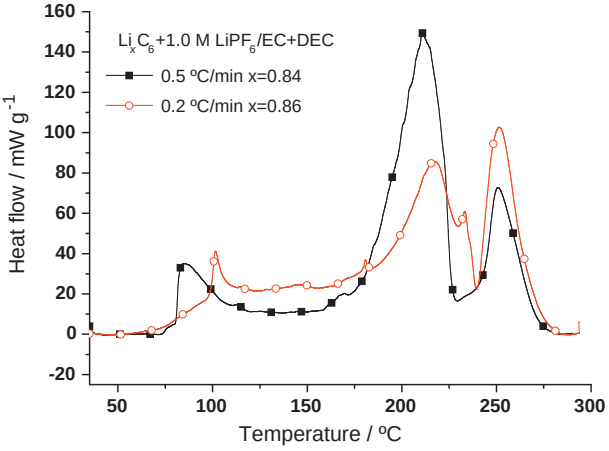

Fig. 9. Heat flows of Li_xC_6–1.0 M $LiPF_6$/EC + DEC at 0.5 and 0.2 °C min^{-1} heating rate.

generation increases with the electrolyte increasing, which may be caused by the decomposition of superfluous electrolyte. The apparent activation energies are close for the 1.6:1, 1:1 and 1:2.4 mass ratios of Li_xC_6–1.0 M $LiPF_6$/EC + DEC based on the original plots, they are 87.0 kJ mol^{-1}, 78.6 kJ mol^{-1} and 97.2 kJ mol^{-1} for the first exothermic process, respectively. However, at 1:3.2 mass ratio the activation energy increase to 154.5 kJ mol^{-1}. The activation energies calculated from the deconvoluted plots are higher than that of original one. In the coupled plots, at the beginning of plots, the heat generation is contributed by several reactions not one reaction in stead, which provides the extra energy to drive the reaction and as a result make the reaction more easily to occur. That is why the apparent activation energies obtained from the original plots are lower than that obtained from the deconvoluted plots.

3.3. *Heating rate effect on the thermal behavior of $Li_{0.5}CoO_2$-electrolyte coexisting system*

Fig. 8 shows the thermal behavior of $Li_{0.5}CoO_2$–1.0 M $LiPF_6$/EC + DEC at 0.5 °C min^{-1}, 0.2 °C min^{-1} and 0.1 °C min^{-1} heating rate. When the heating rate is 0.5 °C min^{-1}, it starts to release heat at 150 °C, and reaches three exothermic peaks at 197 °C, 207 °C and 231 °C with total heat generation of −1084.7 J g^{-1}. At 0.2 °C min^{-1} heating rate, it starts to release heat at 134 °C, followed by three exothermic peaks at 196 °C, 205 °C and 230 °C with total heat generation of −1052.6 J g^{-1}. At slower heating rate of 0.1 °C min^{-1}, the onset temperature decreases to 125 °C, and the corresponding exothermic peaks locate at 171 °C, 181 °C, 188 °C and 216 °C with total heat generation of −577.3 J g^{-1}. It can be speculated that the lower heating rate brings the lower onset temperature, the lower exothermic peak temperatures and less heat generation. In C80 detection system, the lower heating rate means the smaller data detect frequency at the same temperature rise range, for example, at 0.5 °C min^{-1} and 0.2 °C min^{-1} heating rate from 30 °C to 300 °C, the C80 capture one data at every 6.9 s and 16.7 s, respectively, that is the frequencies are 0.1449 and 0.0599, respectively. If the frequency is too small, the data at time $(t_i + t_{i+1})/2$ cannot be real revealed by the data at time t_i and t_{i+1} in the formula of $(f_{ti} + f_{ti+1})/2$. It may be higher or lower than the real reaction, which depends on the reaction process itself. The smaller frequency, the more heat is lost, that is why the lower heating rate could cause less heat generation.

3.4. *Heating rate effect on the thermal behavior of Li_xC_6-electrolyte coexisting system*

Fig. 9 shows the thermal behavior of Li_xC_6–1.0 M $LiPF_6$/EC + DEC at 0.5 °C min^{-1} and 0.2 °C min^{-1} heating rate. At the 0.5 °C min^{-1} heating rate, the $Li_{0.84}C_6$–1.0 M $LiPF_6$/EC + DEC coexisting system starts to release heat at 73 °C, which is 13 °C higher than that of 0.2 °C min^{-1} heating rate. However, it reaches the exothermic peak temperature at 85 °C with heat generation of −121.3 J g^{-1}, which

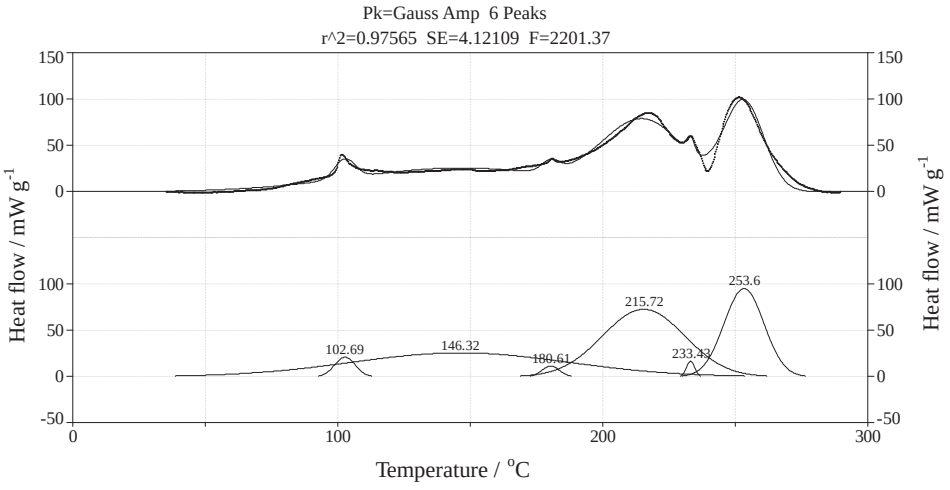

Fig. 10. Deconvoluted C80 plots of heat flow as a function of temperature for Li_xC_6 and 1.0 M $LiPF_6$/EC + DEC electrolyte at 1:1 mass ratio at 0.5 °C min^{-1} heating rate.

Table 6
Thermodynamics and kinetics of Li_xC_6 and 1.0 M $LiPF_6$/EC + DEC electrolyte at 1:1 mass ratio at 0.5 °C min^{-1} heating rate.

Li_xC_6-electrolyte 1:1 mass ratio	Peak temp. (°C)	Reaction heat ($J\,g^{-1}$)	Activation energy E ($kJ\,mol^{-1}$)	Pre-exponential factor A (s^{-1})	Relativity R^2
Peak a	102.7	−24.6	332.87	2.60×10^{43}	0.98397
Peak e	146.3	−318.4	40.37	1.84×10^{2}	0.99475
Peak f	180.6	−11.5	741.60	5.38×10^{82}	0.98162
Peak b	215.7	−340.0	208.49	1.50×10^{19}	0.9912
Peak c	233.4	−7.7	1980.57	7.54×10^{201}	0.97475
Peak d	253.6	−215.1	370.72	4.61×10^{33}	0.98037
Total		−917.3			

is 17 °C lower than that of 0.2 °C min^{-1} heating rate. It reaches to the second and third exothermic peaks at 211 °C and 251 °C with heat generation of −616.0 $J\,g^{-1}$ and −193.3 $J\,g^{-1}$, respectively. In the deconvoluted plots shown in Fig. 10, another two exothermic peaks were picked similar with the one at 0.2 °C min^{-1} heating rate. The thermodynamic and kinetics parameters are listed in Table 5 and Table 6. When the heating rate is high, may be the first stage reaction not be finished, and then it passes to the next reaction, that is why the Li_xC_6–$LiPF_6$/EC + DEC coexisting system generates lower reaction heat under higher heating rate. Furthermore, at the 0.5 °C min^{-1} heating rate, the coexisting system shows large activation energy value.

4. Conclusions

The $Li_{0.5}CoO_2$–$LiPF_6$/EC + DEC coexisting system shows one to four main exothermic processes at the mass ratios of 2:1, 1:1, 1:2 and 1:3 at elevated temperature, respectively. However, when the masses of $Li_{0.5}CoO_2$ and electrolyte are close to each other, the heat generations are close too. If the mass difference is large, such as the mass ratio $Li_{0.5}CoO_2$ with electrolyte is 1:3, the heat generation increases 631.9 $J\,g^{-1}$ than that of the mass ratio is 1:1. Therefore, it is better to use fewer electrolytes at the condition of meeting the electrochemical performance of the lithium ion battery. For this coexisting system, the lower heating rate, the lower onset temperature and lower exothermic peak temperatures. The lower heating rate the less heat generation for the $Li_{0.5}CoO_2$–$LiPF_6$/EC + DEC coexisting system also was observed.

The changes of mass ratio plays less effect on the onset temperature of the coexisting system, they are start to release heat near 58 °C, and the exothermic peaks are almost same except the one with 1:3.2 mass ratio of Li_xC_6–1.0 M $LiPF_6$/EC + DEC. The heat generation is increasing with the mass content increasing of electrolyte, which is caused by the superfluous electrolyte.

Acknowledgements

This study was supported by Scientific Research Foundation for Returned Overseas Scholars, Program for New Century Excellent Talents in University and the Fundamental Research Funds for the Central Universities, Ministry of Education of PR China. Thanks for the reviewer's comments on the deconvolution method to analysis the heat flow plots.

References

[1] T. Horiba, T. Maeshima, F. Matsumura, M. Koseki, J. Arai, Y. Muranaka, J. Power Sources 146 (2005) 107–110.
[2] in: Sciencin: ScienceDaily, American Chemical Society, 2007, pp. eDaily, American Chemical Society, 2007, pp. http://www.http://www.sciencedaily.com/releases/2007/2012/071217110106.htmsciencedaily.com/releases/2007/2012/071217110106.htm.
[3] S. Tobishima, J. Yamaki, J. Power Sources 82 (1999) 882–886.
[4] P. Biensan, B. Simon, J.P. Peres, A. de Guibert, M. Broussely, J.M. Bodet, F. Perton, J. Power Sources 82 (1999) 906–912.
[5] Y. Baba, S. Okada, J. Yamaki, Solid State Ionics 148 (2002) 311–316.
[6] Q.S. Wang, J.H. Sun, X.L. Yao, C.H. Chen, Thermochim. Acta 437 (2005) 12–16.
[7] Q.S. Wang, J.H. Sun, X.L. Yao, C.H. Chen, J. Electrochem. Soc. 153 (2006) A329–A333.
[8] J.R. Dahn, E.W. Fuller, M. Obrovac, U. Vonsacken, Solid State Ionics 69 (1994) 265–270.
[9] D.D. MacNeil, J.R. Dahn, J. Electrochem. Soc. 149 (2002) A912–A919.
[10] M. Ihara, B.T. Hang, K. Sato, M. Egashira, S. Okada, J. Yamaki, J. Electrochem. Soc. 150 (2003) A1476–A1483.
[11] J.W. Jiang, J.R. Dahn, Electrochim. Acta 49 (2004) 4599–4604.
[12] Q. Huang, M.M. Yan, Z.Y. Jiang, J. Power Sources 156 (2006) 541–546.
[13] Y.B. He, Z.Y. Tang, Q.S. Song, H. Xie, Q. Xu, Y.G. Liu, G.W. Ling, Thermochim. Acta 480 (2008) 15–21.
[14] Q.S. Wang, J.H. Sun, C.H. Chen, X.M. Zhou, J. Therm. Anal. Calorim. 92 (2008) 563–566.
[15] Y.S. Park, S.M. Lee, Electrochim. Acta 54 (2009) 3339–3343.
[16] Q.S. Wang, J.H. Sun, X.F. Chen, G.Q. Chu, C.H. Chen, Mater. Res. Bull. 44 (2009) 543–548.
[17] S.H. Kang, K. Amine, J. Power Sources 119 (2003) 150–155.
[18] S.H. Choi, O.A. Shlyakhtin, J. Kim, Y.S. Yoon, J. Power Sources 140 (2005) 355–360.
[19] P.Y. Liao, J.G. Duh, S.R. Sheen, J. Power Sources 143 (2005) 212–218.
[20] I. Belharouak, Y.K. Sun, W. Lu, K. Amine, J. Electrochem. Soc. 154 (2007) A1083–A1087.
[21] Q.S. Wang, J.H. Sun, C.H. Chen, J. Electrochem. Soc. 154 (2007) A263–A267.
[22] K.W. Nam, W.S. Yoon, X.Q. Yang, J. Power Sources 189 (2009) 515–518.
[23] J. Jiang, J.R. Dahn, Electrochim. Acta 49 (2004) 2661–2666.
[24] Q.S. Wang, J.H. Sun, C.H. Chen, J. Power Sources 162 (2006) 1363–1366.
[25] J. Yamaki, Y. Baba, N. Katayama, H. Takatsuji, M. Egashira, S. Okada, J. Power Sources 119 (2003) 789–793.
[26] A.M. Andersson, K. Edstrom, N. Rao, A. Wendsjo, J. Power Sources 82 (1999) 286–290.
[27] M. Herstedt, H. Rensmo, H. Siegbahn, K. Edstrom, Electrochim. Acta 49 (2004) 2351–2359.
[28] M. Holzapfel, F. Alloin, R. Yazami, Electrochim. Acta 49 (2004) 581–589.
[29] L.W. Zhao, I. Watanabe, T. Doi, S. Okada, J. Yamaki, J. Power Sources 161 (2006) 1275–1280.
[30] Y.S. Park, H.J. Bang, S.M. Oh, Y.K. Sun, S.M. Lee, J. Power Sources 190 (2009) 553–557.
[31] Q.S. Wang, J.H. Sun, C.H. Chen, J. Hazard. Mater. 167 (2009) 1209–1214.
[32] J. Yamaki, H. Takatsuji, T. Kawamura, M. Egashira, Solid State Ionics 148 (2002) 241–245.
[33] N.S. Choi, I.A. Profatilova, S.S. Kim, E.H. Song, Thermochim. Acta 480 (2008) 10–14.
[34] L. Gaines, R. Cuenca, Center for Transportation Research Argonne, National Laboratory, Argonne, 2000.
[35] D.D. MacNeil, J.R. Dahn, J. Electrochem. Soc. 148 (2001) A1205–A1210.
[36] Q. Huang, M. Yan, Z. Jiang, J. Solid State Electrochem. 12 (2008) 671–678.
[37] M. Elsabee, R.J. Prankerd, Int. J. Pharm. 86 (1992) 211–219.
[38] T. Boddington, H.A. Chia, P. Halfordmaw, H.T. Feng, P.G. Laye, Thermochim. Acta 195 (1992) 365–372.
[39] H.Y. Wang, M. Yoshio, J. Power Sources 195 (2010) 389–392.
[40] P. Georen, G. Lindbergh, J. Power Sources 124 (2003) 213–220.
[41] Q.S. Wang, J.H. Sun, X.L. Yao, C.H. Chen, J. Loss. Prevent. Proc. 19 (2006) 561–569.
[42] Q.S. Wang, J.H. Sun, X.L. Yao, C.H. Chen, J. Solution Chem. 35 (2006) 179–189.